

Global Biogeochemical Cycles

RESEARCH ARTICLE

10.1002/2017GB005829

Key Points:

- Newly formed Labrador Sea Water was consistently -6.1% to -7.6% undersaturated in oxygen when convection was deeper than 800 m
- Oxygen was more undersaturated for deeper convection or convection ending earlier, resulting in a predictive relationship
- Lateral input of low oxygen waters during restratification provides evidence that the Labrador Sea is a region of net oxygen uptake

Supporting Information:

- Supporting Information S1

Correspondence to:

M. K. Wolf,
mkwolf@uvic.ca

Citation:

Wolf, M. K., Hamme, R. C., Gilbert, D., Yashayaev, I., & Thierry, V. (2018). Oxygen saturation surrounding Deep Water formation events in the Labrador Sea from Argo-O₂ data. *Global Biogeochemical Cycles*, 32, 635–653. <https://doi.org/10.1002/2017GB005829>

Received 27 OCT 2017

Accepted 22 MAR 2018

Accepted article online 25 MAR 2018

Published online 19 APR 2018

Corrected 3 MAY 2018

This article was corrected on 3 MAY 2018. See the end of the full text for details.

Oxygen Saturation Surrounding Deep Water Formation Events in the Labrador Sea From Argo-O₂ Data

Mitchell K. Wolf¹ , Roberta C. Hamme¹ , Denis Gilbert² , Igor Yashayaev³ , and Virginie Thierry⁴ 

¹School of Earth and Ocean Sciences, University of Victoria, Victoria, British Columbia, Canada, ²Maurice-Lamontagne Institute, Fisheries and Oceans Canada, Mont-Joli, Quebec, Canada, ³Bedford Institute of Oceanography, Fisheries and Oceans Canada, Dartmouth, Nova Scotia, Canada, ⁴Ifremer, Laboratoire d'Océanographie Physique et Spatiale, Plouzané, France

Abstract Deep water formation supplies oxygen-rich water to the deep sea, spreading throughout the ocean by means of the global thermohaline circulation. Models suggest that dissolved gases in newly formed deep water do not come to equilibrium with the atmosphere. However, direct measurements during wintertime convection are scarce, and the controls over the extent of these disequilibria are poorly quantified. Here we show that, when convection reached deeper than 800 m, oxygen in the Labrador Sea was consistently undersaturated at -6.1% to -7.6% at the end of convection. Deeper convection resulted in greater undersaturation, while convection ending later in the year resulted in values closer to equilibrium, from which we produce a predictive relationship. We use dissolved oxygen data from six profiling Argo floats in the Labrador Sea between 2003 and 2016, allowing direct observations of wintertime convection. Three of the six optode oxygen sensors displayed substantial average in situ drift of $-3.03 \mu\text{mol O}_2 \text{ kg}^{-1} \text{ yr}^{-1}$ ($-0.94\% \text{ O}_2 \text{ yr}^{-1}$), which we corrected to stable deepwater oxygen values from repeat ship surveys. Observations of low oxygen intrusions during restratification and a simple mixing calculation demonstrate that lateral processes act to lower the oxygen inventory of the central Labrador Sea. This suggests that the Labrador Sea is a net sink for atmospheric oxygen, but uncertainties in parameterizing gas exchange limit our ability to quantify the net uptake. Our results constrain the oxygen concentration of newly formed Labrador Sea Water and allow more precise estimates of oxygen utilization and nutrient regeneration in this water mass.

Plain Language Summary The surface ocean and the atmosphere constantly exchange gases with each other. In many regions, this exchange brings dissolved gases close to equilibrium with the atmosphere. However, wintertime convection carries water low in oxygen from the deep ocean to the surface. The ocean may not be able to exchange oxygen with the atmosphere quickly enough to reach equilibrium before convection ends. Here we show that, in the Labrador Sea, deeper convection resulted in dissolved oxygen further from equilibrium, while convection lasting later in the year resulted in dissolved oxygen closer to equilibrium. From the depth and end date of convection, we can predict how close oxygen levels will be to equilibrium. Because bad weather prevents shipboard observations of most convection events, we use dissolved oxygen data from six robotic Argo floats that collect measurements from 2,000 m to the surface every 10 days. After convection, we observe water with low oxygen moving into the central Labrador Sea from surrounding areas. This suggests that, overall, the Labrador Sea takes up more oxygen from the atmosphere than it releases. Our results enable a better understanding of oxygen dynamics during convection and allow more precise estimates of oxygen consumption in the deep ocean.

1. Introduction

Deep water formation is important because it is the mechanism by which the deep ocean communicates with the atmosphere, facilitating exchanges of heat and important gases such as carbon dioxide and oxygen (Azetsu-Scott et al., 2003; DeGrandpre et al., 2006; Lab Sea Group, 1998). The large wintertime heat loss in these regions induces deep convection, which drives ocean uptake of carbon dioxide and oxygen, while export of newly formed deep water redistributes dissolved gases from the poles to low latitudes and influences global climate (Lazier et al., 2002). Our study focuses on the Labrador Sea, a key region for uptake of anthropogenic carbon (Khatriwala et al., 2013), which slows the rise of atmospheric carbon dioxide (Sabine et al., 2004; Steinfeldt et al., 2009) but also increases ocean acidification (Azetsu-Scott et al., 2010). High-

latitude warming in response to climate change may strengthen stratification in the Labrador Sea (Böning et al., 2016; Dickson et al., 2007), reduce deep water formation and the amount of carbon dioxide uptake, and decrease deep ocean oxygen as has been observed in intermediate waters around the world (Gilbert, 2017; Gilbert et al., 2010; Keeling et al., 2010). Since there are no internal sources of oxygen below the euphotic zone, reduced deep water formation would disrupt crucial deep-sea habitats and change the preservation of organic material in sediments through oxygen deprivation (Cowie et al., 1995).

In this study, we determine the oxygen content of Labrador Sea Water, newly formed by local winter convection, and quantify net oxygen uptake. Unlike most of the world's surface ocean where dissolved oxygen is close to equilibrium (Broecker & Peng, 1982; Najjar & Keeling, 1997), deep convection regions do not fully equilibrate with the atmosphere (Clarke & Coote, 1988). Biological respiration creates an oxygen deficit in deeper waters, which can be further transported to other regions. Convection mixes this low-oxygen deep water to the surface. During deep water formation in the Labrador Sea, the entrainment of low oxygen water into the mixed layer and subsequent mixing and sinking happens on a faster timescale than the counteracting air-sea gas exchange, so the undersaturated surface water sinks before it can fully equilibrate (Körtzinger et al., 2008).

Quantifying the extent of surface oxygen disequilibria, as presented below, will improve studies using apparent oxygen utilization (AOU) to determine respiration and regenerated nutrients in the ocean interior (Carlson et al., 2010; Duteil et al., 2012, 2013). AOU is meant to quantify oxygen consumption since the water was last at the surface and typically assumes that surface ocean oxygen is at equilibrium with the atmosphere everywhere. However, most of the ocean interior was last at the surface at high latitudes, such as the Labrador Sea, during winter when surface waters are typically undersaturated in oxygen. Model results show that AOU likely overestimates oxygen consumption by respiration by 10–30 $\mu\text{mol kg}^{-1}$ in the deep North Atlantic, a large proportion of the $<100 \mu\text{mol kg}^{-1}$ AOU signal observed in these waters (Duteil et al., 2013; Ito et al., 2004). These model results need confirmation by direct observations of surface oxygen disequilibria, also known as preformed oxygen, during deep water formation events, but such observations are scarce. Our study's preformed oxygen values will provide a correction to AOU estimates in Labrador Sea Water, an important component of North Atlantic Deep Water.

The Labrador Sea, our study site, is one of the most thoroughly studied deep-convection regions in the world (e.g., Kieke & Yashayaev, 2015, and references within). This area is influenced by strong physical and biological forcings centered around the cyclonic subpolar gyre in the North Atlantic (Lab Sea Group, 1998). The central Labrador Sea is characterized by doming isopycnals that are weakly stratified due to deep winter convection, forming Labrador Sea Water. Successive years of winter convection can precondition the water column for extremely deep convection by weakening stratification (Yashayaev & Loder, 2017). Cold, dry air coming from the Canadian continent fuels winter mixing and removes heat from the Labrador Sea (Schulze et al., 2016). This mixing resupplies the surface waters with nutrients, driving the spring phytoplankton bloom. In the winter, convection occurs in localized, short-lived convective plumes on the order of 1 km, which are mixed by mesoscale eddies to form large homogenized patches within the Labrador Sea (Lab Sea Group, 1998; Piron et al., 2016, 2017; Steffen & D'Asaro, 2002). The deepest convection is typically seen in the southwestern region. Piron et al. (2016) observed that restratification in the Irminger Sea took place almost simultaneously over a large area, and the same likely occurs in the Labrador Sea. The complex interplay between atmospheric forcing and preconditioning resulting in Labrador Sea deep convection (Yashayaev & Loder, 2017) leads to strong interannual variability, with convection depths ranging from less than 600 m to greater than 1,700 m (Piron et al., 2017; Yashayaev, 2007; Yashayaev & Loder, 2016). If this interannual variability affects how closely oxygen approaches equilibrium, varying deep water formation events will create waters with varying oxygen concentrations, density, and other properties (Yashayaev & Loder, 2016).

We make use of autonomous platforms carrying oxygen sensors as an important resource for investigating deep convection, because only a handful of ship-based oxygen measurements have been made during the Labrador Sea's deep convection period due to rough seas (Clarke & Coote, 1988; Zimmerman et al., 2000). Profiling floats equipped with oxygen sensors have significantly increased dissolved oxygen measurements in the ocean since the early 2000s (Johnson et al., 2009) and are planned to increase further with the Biogeochemical-Argo Program (Biogeochemical-Argo Planning Group, 2016). Over 800 Argo floats have been equipped with oxygen sensors (Argo, 2000). Typically, these floats drift at 1,000 m for 10 days, then sink to

2,000 m before rising to the surface. As they ascend, they take in situ measurements of dissolved oxygen, salinity, and temperature. This cycle is repeated every 10 days for the float's lifetime, ~4 years. Dissolved oxygen profiles from Argo floats have been used to understand ocean-atmosphere processes such as air-sea gas exchange (Kihm & Körtzinger, 2010) and ocean ventilation/oxygen inventory gain during deep convection (Körtzinger et al., 2004; Piron et al., 2016, 2017), biogeochemical processes such as carbon export (Martz et al., 2008) and net community production (Plant et al., 2016; Riser & Johnson, 2008), and the stability of oxygen minimum zones (Prakash et al., 2012). Moorings equipped with oxygen sensors have also been used to study the oxygen inventory gain and air-sea flux during deep convection in the Labrador Sea (Koelling et al., 2017) and to describe the seasonal cycle of oxygen (Körtzinger et al., 2008).

In this study, we use oxygen data from Argo-O₂ floats to investigate how competing oceanic processes during deep convection affect how closely oxygen concentrations approach equilibrium by the end of convection. In addition, strong interannual variability of convection in the Labrador Sea (Yashayaev, Bersch, & vanAken 2007; Yashayaev & Loder, 2016) motivates us to determine how the degree of equilibration varies from year to year, particularly with respect to the depth and end date of convection. In section 2, we describe our methods including float details, data processing, and calculations. In section 3, we describe our technique to calibrate oxygen optode sensors to stable deepwater oxygen values from repeat hydrography. In section 4, we examine the seasonal cycle of oxygen and the processes affecting the end of convection oxygen values, particularly depth and end date of convection, followed by investigating net oxygen uptake from a comparison of air-sea and lateral fluxes to the observed oxygen inventory.

2. Methods and Data Sources

2.1. Data Selection

We used dissolved oxygen data from 6 Argo floats (Argo, 2000) active in the Labrador Sea between 2003 and 2016 (Table 1), resulting in 15 individual float-year observations of wintertime convection. We selected floats that spent multiple winters in the Labrador Sea with regular profiles to 2,000 m. We excluded 6 other Canadian Argo-O₂ floats in the Labrador Sea, because three were confined to the boundary currents (4900879, 4900880, and 4901141), while the other three, despite spending some time in the central Labrador Sea, never observed winter convection (4901142, 4901780, and 4901782). We focused our study on the region in the Labrador Sea where deep convection is most likely to occur (black boundary in Figure 1), based on the observed region of weak stratification and maximum buoyancy loss (Lab Sea Group, 1998) as well as the 2,500-m isobath. Float profiles outside this region were excluded from the analysis. Although convection depth is not uniform across our study region, using multiple floats within this region produces a representative picture of the conditions across the Labrador Sea.

All oxygen data used in this study come from Aanderaa optodes, model 3830 for the three older floats and model 4330 for the three newest floats (Table 1). Both models use dynamic quenching, measuring the phase shift in the fluoresced excitation signal occurring when oxygen interacts with the luminophores within the sensing foil. Except for float 6901030, for which oxygen concentration was calculated from phase at the national Argo data center following Thierry et al. (2016), optode oxygen concentrations were calculated internally using this phase shift, optode-measured temperature, and an internal reference salinity (Tengberg et al., 2006). The data available from the Global Argo data center for all these floats were as a concentration, not phase. Section 3 describes calibration of all float oxygen data.

2.2. Pressure and Salinity Corrections

Upon data acquisition, raw dissolved oxygen values from floats 1901210, 1901217, 6901030, and 4900494 were corrected for pressure (Uchida et al., 2008) and salinity effects at the Argo National Data Centers according to the "Processing Argo OXYGEN data at the DAC level, Version 1.3" manual (Thierry et al., 2013). We updated the pressure correction to that recommended by Bittig et al. (2015) according to the "Processing Argo OXYGEN data at the DAC level, Version 2.2" manual (Thierry et al., 2016). This new pressure correction gives constant oxygen concentrations from the surface to the bottom of deeply convecting layers, while the old correction showed average changes of $3.14 \mu\text{mol kg}^{-1}/1,000 \text{ m}$ (Figure S1 in the supporting information). Floats 4900611 and 4900607 had no pressure or salinity corrections applied at the time of data acquisition. We applied the pressure correction recommended by Bittig et al. (2015) and salinity correction

Table 1
Argo Float Information for All Floats Used in This Study

Float ID	Data center ^a	PI name	Date of first profile in study region	Sensor model	Drift rate ^b in $\mu\text{mol kg}^{-1} \text{yr}^{-1}$ ($\text{So}_2\% \text{yr}^{-1}$ in parentheses)	Gain equation ^c $G(t) = \text{So}_2^{\text{Deep}}/F(t)$	RMSE ^d of fit ($\text{So}_2[\%]$)
1901210	IF	Virginie Thierry	25 Jan 2012	Aanderaa Optode 4330	-2.52 (-0.80)	$85.84/(-5.43 \cdot [1 - \exp(-\delta t / 1.66 \times 10^3)] + 80.89)$	0.12
1901217	IF	Virginie Thierry	26 July 2011	Aanderaa Optode 4330	-3.08 (-0.95)	$85.84/(-6.12 \cdot [1 - \exp(-\delta t / 1.20 \times 10^3)] + 80.04)$	0.14
6901030	IF	Virginie Thierry	12 April 2013	Aanderaa Optode 4330	-3.50 (-1.08)	$85.84/(-3.58 \cdot [1 - \exp(-\delta t / 7.46 \times 10^2)] + 80.04)$	0.07
4900494	ME	Blair Greenan	4 June 2004	Aanderaa Optode 3830	-1.12 (-0.35)	$86.35/(-9.50 \times 10^{-4} \cdot \delta t + 88.53)$	0.16
4900611	IF	Jens Schimanski	8 December 2004	Aanderaa Optode 3830	-0.27 (-0.07)	$86.35/(-1.92 \times 10^{-4} \cdot \delta t + 79.34)$	0.12
4900607	IF	Jens Schimanski	14 September 2003	Aanderaa Optode 3830	-1.38 (-0.43)	$87.22/(-1.17 \times 10^{-3} \cdot \delta t + 87.10)$	0.16

^aIF indicates Ifremer, France; ME indicates MEDS, Canada. ^bMean annual drift for an individual float's entire lifespan (see section 3). ^cTime-dependent function that can be multiplied by the float's oxygen saturation values (determined from Argo DOXY values corrected following section 2.2) to obtain calibrated values, where δt is days since first profile in study region. ^dRoot mean square error (RMSE) between the fit function and the float measured oxygen saturation at 1,800–1,900 m

according to the newest processing manual (Thierry et al., 2016), noting that floats 4900611 and 4900607 had internal reference salinities of 35 and 0, respectively. Which version of the processing manual has been used by the DAC for most optode floats in the Argo database remains unclear; we recommend inquiring with the respective float principal investigators when necessary.

2.3. Convection End Date

We needed to define the convection end date for each float-year to investigate the oxygen saturation anomaly at the end of convection (section 4.2). Choosing the convection end date was done visually by inspecting individual profiles of temperature, salinity, potential density, dissolved oxygen, and oxygen saturation anomaly on a float-by-float and year-by-year basis (Wolf, 2017). We chose the convection end date as the profile with the deepest mixed layer where subsequent profiles showed either restratification in the upper-layer waters or replacement of middepth waters through horizontal advection/changing float position. We also considered convection duration as a metric. However, determining the convection start date was more subjective, and our results were robust to the choice of convection end date versus convection duration (Wolf, 2017).

2.4. Oxygen Saturation

We use both oxygen saturation and oxygen saturation anomaly in this paper. These represent the deviation of oxygen concentrations from equilibrium that drives the air-sea oxygen flux, controlling how much oxygen uptake or outgassing occurs. Oxygen saturation (So_2) is the ratio (as a percent) of measured oxygen concentration to the oxygen concentration of water at equilibrium with the atmosphere based on potential temperature and salinity, while the oxygen saturation anomaly (ΔO_2) is calculated by subtracting 100% from the oxygen saturation. We use both terms, because the optode calibration equations are most easily fit to saturation, whereas saturation anomaly is more intuitive when discussing the ocean as a net sink (negative ΔO_2) or net source (positive ΔO_2) of oxygen during air-sea gas exchange.

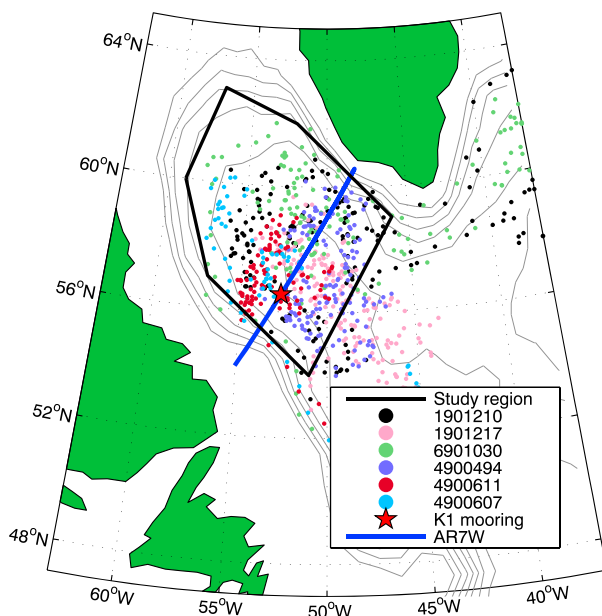


Figure 1. Locations of individual float profiles from the six floats chosen for this study with float numbers indicated in legend. The black line indicates our analysis region. The red star indicates the K1 mooring location. The blue line indicates the AR7W hydrographic line. The gray lines indicate bathymetry at 500-m intervals, starting at 1,000 m.

$$S_{O_2} = \left(\frac{[O_2]_{float}}{[O_2]_{eq}} \right) \cdot 100\% \quad , \quad \Delta O_2 = \left(\frac{[O_2]_{float}}{[O_2]_{eq}} - 1 \right) \cdot 100\% \quad (1)$$

where $[O_2]_{float}$ is the oxygen concentration measured by the float, and $[O_2]_{eq}$ is the oxygen concentration at equilibrium with 1-atm pressure calculated using Garcia and Gordon (1992, 1993) and float-measured potential temperature and salinity. These saturations are those the water would have at the surface, neglecting the hydrostatic pressure effect on gas solubility (Hamme et al., 2015; Klots, 1961).

2.5. Air-Sea Oxygen Flux

To assess some of the uncertainty, we calculated the air-sea oxygen flux using two gas exchange parameterizations incorporating bubbles as well as two wind speed products. Bubbles are an important air-sea gas exchange mechanism for insoluble gases like oxygen (Woolf, 1997; Woolf & Thorpe, 1991), particularly in the Labrador Sea (Sun et al., 2017). We chose the Liang et al. (2013) and Yang et al. (2017) parameterizations over others that include bubbles (e.g., Stanley et al., 2009; Vagle et al., 2010; Woolf, 1997; Woolf & Thorpe, 1991), because the Liang et al. (2013) parameterization best reproduces noble gas observations, which are highly affected by bubbles (Emerson & Bushinsky, 2016), and matches annual net community production rates determined from oxygen data to rates from nitrate data (Plant et al., 2016). The Yang et al. (2017) parameterization is an optimization of the Liang et al. (2013) parameterization to best reproduce nitrogen concentrations measured by a gas tension device. Our aim is not to compare a variety of gas exchange parameterizations, so we only use Liang et al. (2013) and Yang et al. (2017), and also compare to the most well used parameterization that does not include bubble fluxes, Wanninkhof (1992).

The Liang et al. (2013) and Yang et al. (2017) parameterizations include three flux components: diffusive gas exchange across the air-sea interface (F_S), bubbles that completely dissolve (F_C), and bubbles that partially dissolve (F_P). See also Emerson and Bushinsky (2016) for a comprehensive description of the Liang et al. (2013) parameterization. The three flux components are parameterized from wind speed, the Schmidt number of oxygen which incorporates gas diffusivity, and the air-sea oxygen gradient. We used 6-hr cross-calibrated multiplatform (CCMPv2) surface vector winds on a 0.25° grid (Atlas et al., 2011; Wentz et al., 2015) and 3-hr North American Regional Reanalysis (NARR) surface vector winds on a 32-km grid (Mesinger et al., 2006), with both wind speed products nearest-neighbor interpolated to the float trajectory at the temporal resolution of the wind speeds. Oxygen Schmidt numbers were calculated from Ferrell and Himmelblau (1967) and Sharqawy et al. (2010). Surface float oxygen concentrations were linearly interpolated to either the 6-hourly or 3-hourly wind speed time stamps. Equilibrium oxygen concentrations were calculated from Garcia and Gordon (1992, 1993) using float-measured surface temperature and salinity and corrected for atmospheric pressure by $(P_{slp} - P_{vapor}) / (1 - P_{vapor})$ using 6-hourly sea level pressures (P_{slp}) from NCEP/NCAR Reanalysis I (Kalnay et al., 1996) that were linearly interpolated to the float trajectory and water vapor pressure at saturation (P_{vapor}) from Dickson et al. (2007).

2.6. Column-Integrated Oxygen Inventory

To investigate the change in oxygen inventory in the Labrador Sea, we linearly interpolated the float data to a 1-m depth grid from 0 to 1,900 m and then vertically integrated a 1 m × 1 m × 1,900-m column. Although Argo floats typically measure to 2,000 m, we excluded the deepest 100 m because several profiles show an unlikely “hook” in the oxygen data at the deepest 50 m trending toward low oxygen values, possibly a measurement before the float begins ascending contaminated by particle/bio fouling (Wolf, 2017). Argo floats typically take surface measurements at 4–6 m, so these values were extended up to 0 m during gridding. Float profiles that did not reach shallower than 10 m or started shallower than 1,900 m were excluded from inventory calculations. Profiles that did not reach shallower than 10 m were excluded from all other analyses.

3. Oxygen Sensor Calibration

All oxygen optodes used in this study needed in situ calibration beyond the initial factory calibration. Typically, optodes report lower values relative to the World Ocean Atlas 2009 climatology (Takeshita

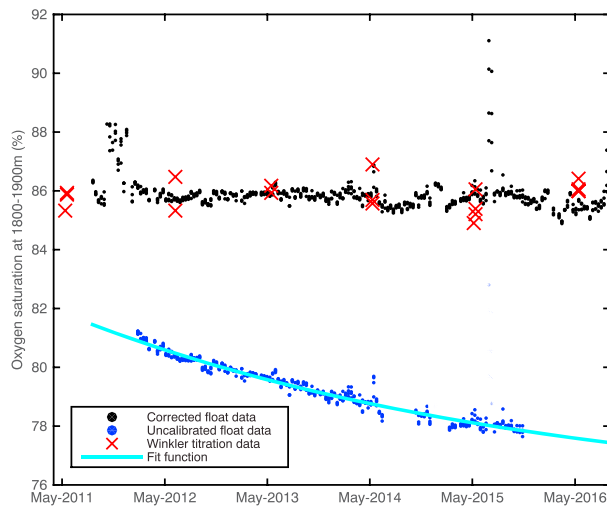


Figure 2. Float 1901210 corrected oxygen saturation (%) at 1,800 to 1,900 m (black dots) compared to the uncalibrated float data for the same depths used for the fit calculation (blue dots). The exponentially decaying fit function (light blue line) is calculated from equation (2). Winkler titration data from annual May surveys of the AR7W hydrographic line are shown in red “x”. All floats shown in Figure S2.

et al., 2013) with mean errors of $\sim 10 \mu\text{mol kg}^{-1}$ (Johnson et al., 2015). This could be due to the prevalent optode “storage drift” in which calibration changes between leaving the factory and field deployment (D’Asaro & McNeil, 2013; Körtzinger et al., 2005; Uchida et al., 2008) or inaccurate initial calibration, but we also detect significant drift post deployment.

We chose to calculate a time-dependent gain for each optode based on relatively stable deep-layer ship-based observations, which corrects for both initial “storage drift” and postdeployment drift. Some past studies suggested that optodes on Argo floats had no detectable in situ drift once deployed (Bittig & Körtzinger, 2015; Takeshita et al., 2013). However, three of the six optodes in this study drifted downward at $>2.5 \mu\text{mol kg}^{-1} \text{ yr}^{-1}$ at concentrations of $277 \mu\text{mol kg}^{-1}$ ($>0.8\% \text{ yr}^{-1}$ at saturations of 86%) after deployment (Table 1), similar to recent studies by Bushinsky et al. (2016) and Bittig and Körtzinger (2017). If left uncorrected, the average in situ drift (with storage drift removed) for these three optodes of $-3.03 \mu\text{mol kg}^{-1} \text{ yr}^{-1}$ would result in average wintertime (December to April) air-sea oxygen flux estimations 17% higher than drift corrected float data in just the float’s first year, with the overestimation rising to 52% in the subsequent year. This postdeployment drift is the primary reason we chose to calibrate optode data relative to deep ocean oxygen saturations rather than a single deployment ship-based profile. Furthermore, since

Argo floats typically profile only every 10 days, ship-based profiles that coincide with both the location and time of float profiles were sometimes not available (Wolf, 2017). Repeat observations over several years of a slow-changing and relatively uniform deep layer provide more time points for comparison between ship-based and float measurements and reduces the potential for bias from a single cruise. Another advantage of our deep-layer calibration technique is that it can be applied postdeployment and does not require special hardware such as the ability to make in-air oxygen measurements (Bittig & Körtzinger, 2015; Bushinsky et al., 2016; Johnson et al., 2015). A disadvantage of this technique, however, is that it depends on the assumption of a stable, temporally invariant pressure effect on the optode to apply the correction to shallower values, which is still under investigation (Bittig et al., 2015; Bittig & Körtzinger, 2017).

Since winter convection in the Labrador Sea during 1994–2015 did not reach below 1,800 m, the layer between 1,800 and 1,900 m shows remarkably weak year-to-year changes in temperature, salinity, and dissolved oxygen. From annual May surveys of the AR7W hydrographic line by Fisheries and Oceans Canada (Figure 1), oxygen values averaged in the 1,800–1,900 m layer of the Labrador Sea remain fairly constant from 2003 to 2016, with mean oxygen concentration $276.5 \pm 2.5 \mu\text{mol kg}^{-1}$ and saturation of $86.0 \pm 0.7\%$ (red “x” in Figure 2). Temperature in this layer rose from $3.03 \pm 0.09 \text{ }^\circ\text{C}$ in 2003–2005 to $3.34 \pm 0.17 \text{ }^\circ\text{C}$ in 2014–2016. The 1,800 to 1,900-m layer mainly contains a mixture of remnant Labrador Sea Water formed during extremely deep convection in the mid-1990s and Icelandic Slope Water (Yashayaev, 2007; Yashayaev, Bersch, & vanAken, 2007; Yashayaev, vanAken, Holliday, & Bersch, 2007). These cruise oxygen data have undergone a thorough quality check, validation, and postcruise revision and have been processed to the WOCE/CLIVAR/GO-SHIP standards of precision and replicate agreement (Culberson, 1994).

For all six optodes used in this study, we fit a function to the float oxygen saturation measurements at 1,800–1,900 m and calculated a time-dependent gain relative to the average oxygen observed in the stable deep layer during an individual float’s lifetime. Although the D’Asaro and McNeil (2013) calibration was designed for storage drift, we observed a similar exponentially decaying shape in the in situ drift for three of the six optodes used in this study (all Aanderaa 4330 optodes); therefore, for these optodes, we used an exponentially decaying fit function. A linear fit function best represented the remaining 3 optodes (all Aanderaa 3830 optodes) and was used to calculate our time-dependent gain function for those optodes. All functions were fit to oxygen saturation rather than saturation anomaly. The exponentially decaying function, $F_{e-fit}(t)$, had the form (D’Asaro & McNeil, 2013):

$$F_{e-fit}(t) = C_0 \cdot \left(1 - e^{-\frac{\delta t}{C_1}}\right) + C_2 \quad (2)$$

while the linear fit function, $F_{l-fit}(t)$, had the form:

$$F_{l-fit}(t) = C_3 \cdot \delta t + C_4 \quad (3)$$

where δt is days since entering the study region. The coefficients C_0 , C_1 , C_2 , C_3 , and C_4 (Table 1) were found by minimizing the sum of the squares of the differences between the fit function and the optode oxygen saturation at 1,800–1,900 m. The average root mean square error (RMSE) of the functions fit to the float measured deep oxygen saturation is 0.13% (Table 1). Float profiles that were outside the study region (Figure 1) or that indicated recently oxygenated waters when convection reached deeper than 1,800 m were excluded from the fit calculation (time gaps for uncalibrated data in Figure 2). We calculated the time-dependant gain, $G(t)$, relative to the stable deep layer observations using:

$$G(t) = \frac{SO_2^{Deep}}{F_{fit}(t)} \quad (4)$$

where SO_2^{Deep} is the mean oxygen saturation in the stable deep layer (1,800 to 1,900 m) calculated only from years spanning the specific float's lifetime (Table 1) and $F_{fit}(t)$ is the fit function determined from equations (2) or (3). We then calculated the final corrected float oxygen saturation, $SO_2^{Float, Corr}$, using:

$$SO_2^{Float, Corr} = G(t) \cdot SO_2^{Float} \quad (5)$$

where SO_2^{Float} is the float uncalibrated oxygen saturation (after corrections following section 2.2). We also considered calibrating using oxygen concentration instead of saturation; however, the difference between the two methods was negligible (Wolf, 2017). We preferred to use saturation, because optodes measure the partial pressure of oxygen, which is linearly related to saturation.

The corrected float oxygen saturation values match the ship-based deep values well (Figure 2). This technique corrects both the initial "storage drift" and in situ drift. Our calibration technique using a single reference depth is essentially a one-point calibration. Multiple studies have shown that a simple gain, rather than a gain and offset, is sufficient to correct optode oxygen values (Bushinsky et al., 2016; D'Asaro & McNeil, 2013; Johnson et al., 2015). For the Labrador Sea, where oxygen concentrations are high and the range in oxygen saturation is relatively small, a similar degree of correction is applied to both surface and deep values. This calibration technique will work best for floats in regions with at least annual repeat hydrography to improve the reliability of ship-based observations, relatively small vertical oxygen gradients to ensure a similar level of correction to the whole profile, and convection depths shallower than 2,000 m (typical Argo profile depth).

Since we calibrate float oxygen data to ship-based observations, we use the associated standard deviation of these ship based measurements ($\pm 2.5 \mu\text{mol kg}^{-1}$ or $\pm 0.7\%$) as the error in our calibrated oxygen data set. Errors of this magnitude can result in a $\pm 24\%$ error in net annual air-sea oxygen fluxes. It is interesting to note that floats deployed after 2010 equipped with Aanderaa 4330 optodes showed significant in situ drift with an exponentially decaying shape, while floats deployed in 2004 and earlier with Aanderaa 3830 optodes showed either no significant in situ drift or a linearly decaying drift (Figure S2). The cause of in situ drift is still speculative, with current theories suggesting a conditioning effect from repeated pressure cycling or removal of surface films and contaminants on the sensing foil (Bittig & Körtzinger, 2017).

We were able to compare the calibration of one of the floats in this study to the calibration of the same float in two other studies. Our calibration of float 4900494 compares well to that of Johnson et al. (2015) for the same float using an in-air calibration method. Many recent optode calibration studies focus on in-air oxygen measurements (Bittig & Körtzinger, 2015; Bittig et al., 2018; Bushinsky et al., 2016; Johnson et al., 2015), which requires the optode to be located where it can sample air when at the surface. The mean surface ΔO_2 difference between the Johnson et al. (2015) calibration and our method for float 4900494 was $0.49 \pm 0.36\%$, with much of the standard deviation arising from the drift during deployment that our method corrects (Wolf, 2017, Appendix I). Although the Johnson et al. (2015) calibration used a constant gain throughout the float's lifetime, the in-air oxygen calibration method is capable of producing a time-dependant gain for drift correction (Bittig et al., 2018;

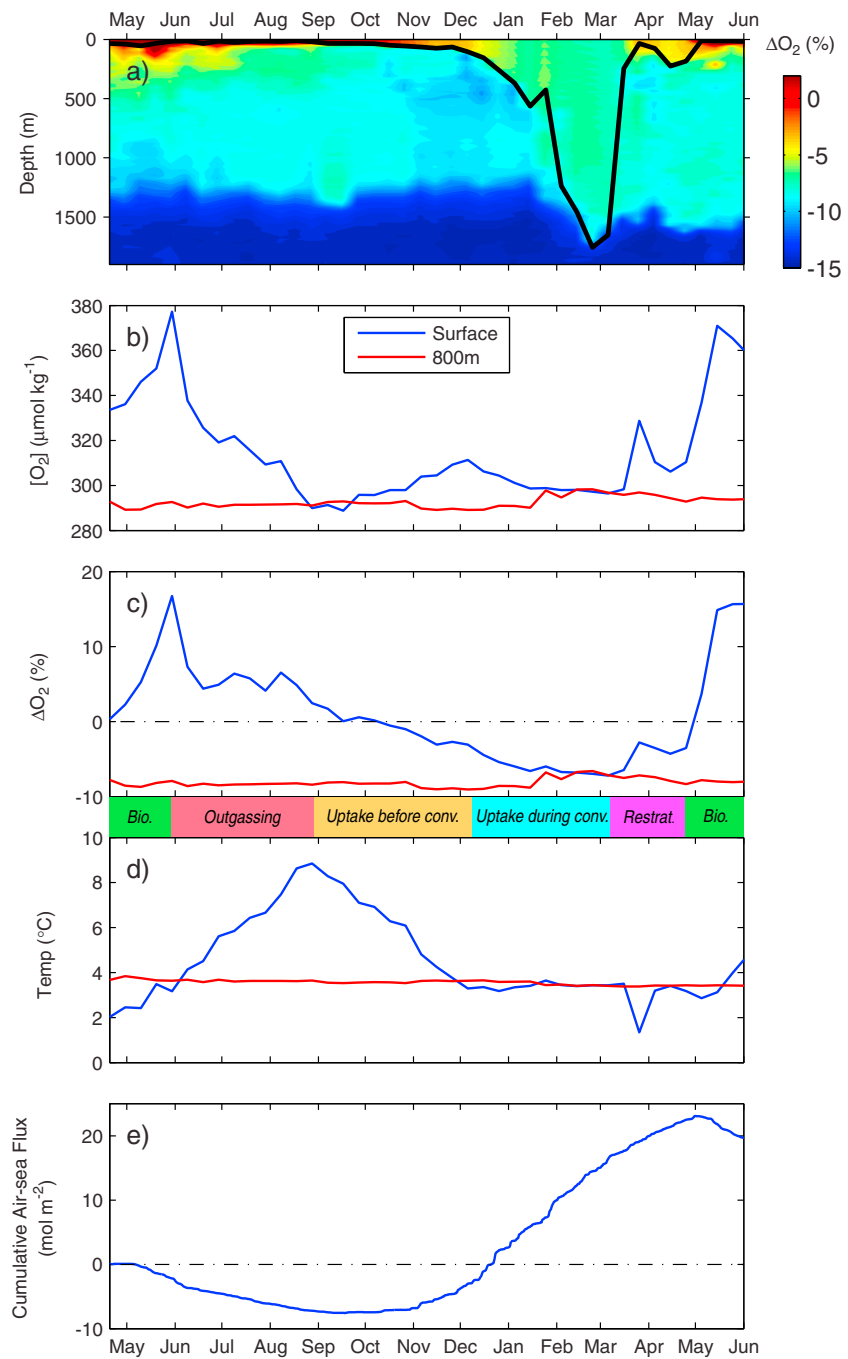


Figure 3. Seasonal cycle from spring 2013 through spring 2014 for float 1901210 of (a) oxygen saturation anomaly (%) in the top 1,900 m, with mixed layer depth (m) from Holte et al. (2016) indicated by the thick black line (b) oxygen concentration ($\mu\text{mol kg}^{-1}$), (c) oxygen saturation anomaly (%), (d) temperature ($^{\circ}\text{C}$), and (e) cumulative air-sea oxygen flux (mol m^{-2}) using the Liang et al. (2013) gas exchange parameterization and CCMPv2 winds. For (b) to (d), the blue lines indicate surface values and the red lines indicate values at 800 m. The colored bar represents time periods of (green) biological activity, (pink) outgassing, (orange) oxygen uptake before convection, (cyan) oxygen uptake during convection, and (purple) restratification.

Bushinsky et al., 2016). Bittig et al. (2018) analyzed this same float including a time-dependent gain. Our first profile gain value of 0.975 and subsequent average annual drift of $-0.35\% \text{ O}_2 \text{ yr}^{-1}$ compares well to the first profile gain value of 0.994 and linear trend of air O_2 observations of $-0.17\% \text{ yr}^{-1}$ from Bittig et al. (2018).

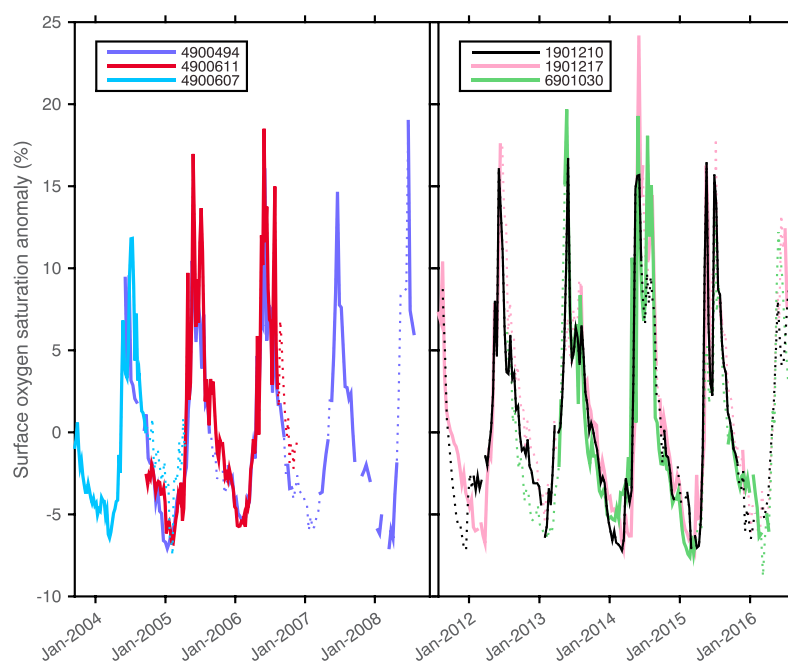


Figure 4. Time series of surface oxygen saturation anomaly (%) for all floats used in this study with float numbers in legend. Profiles without surface measurements in the upper 10 m cause gaps. The years 2009 to late 2011 are removed due to lack of data. The dotted line segments indicate periods when floats drifted outside the region of interest.

4. Results and Discussion

4.1. Surface Annual Cycle

We illustrate the seasonal oxygen cycle in the Labrador Sea using a representative year of data (Figure 3). The spring bloom timing, magnitude, and location vary as a result of physical forcings (freshwater stratification, eddy activity, temperature, and light; Frajka-Williams & Rhines, 2010; Körtzinger et al., 2008; Wu et al., 2008). This bloom drives an increase in surface oxygen concentration and saturation anomaly (green bar in Figure 3). Surface oxygen concentrations can rise by over $50 \mu\text{mol kg}^{-1}$, reaching a saturation anomaly $>15\%$. Surface temperatures remain cool until summer when they rise significantly. The spring bloom oxygen increase and the warming waters induce outgassing of oxygen during summer, resulting in decreasing surface oxygen concentrations tending toward equilibrium (pink bar in Figure 3). Surface temperature reaches its maximum near the end of August, corresponding to the surface oxygen concentration minimum.

During fall before convection, surface temperatures decrease while winds (not shown) increase. As cooling occurs, surface waters become undersaturated and oxygen is taken up (orange bar in Figure 3). This preconditioning weakens the surface stratification, but mixed layers remain shallow with the oxygen concentration increase confined to the surface (Lavender et al., 2002).

During winter, continued heat loss and increased wind speeds deepen the mixed layer (blue bar in Figure 3). At convection's start, water below the mixed layer has a lower oxygen concentration, with an oxygen saturation anomaly of -5% to -8% . As the mixed layer deepens, these oxygen undersaturated deep waters are exposed to the surface, lowering the surface oxygen concentration and saturation anomaly (Lazier et al., 2002; Pickart et al., 2002). This newly exposed undersaturated water takes up oxygen from the atmosphere and is mixed downward, raising the concentration and saturation anomaly of the deep waters. However, heat loss and vertical mixing occur too quickly for air-sea gas exchange to bring the surface water to equilibrium with the atmosphere (Körtzinger et al., 2008), resulting in undersaturated waters at convection's end. After convection, restratification occurs quickly (purple bar in Figure 3) as water from outside the convective region replaces the well-mixed layer at various depths (Frajka-Williams et al., 2014; Körtzinger et al., 2004; Lilly et al., 2003).

Table 2
End of Convection Properties Observed by the Floats Used in This Study^a

Winter year	Float ID	Convection end saturation anomaly (%)	Convection end date	Maximum convection depth from float (m)	Maximum convection depth from literature ^b (m)
2003/2004	4900607	-6.07	21 March 2004	1,000	1,350
2004/2005	4900494	-4.35	31 March 2005	400	1,150
	4900611	-5.34	23 February 2005	600	1,150
2005/2006	4900494	-4.12	16 March 2006	250	1,150
	4900611	-4.58	8 March 2006	700	1,150
2007/2008	4900494	-7.02	15 March 2008	1,590	1,500
2011/2012	1901217	-6.29	13 March 2012	880	1,300
2012/2013	1901210	-5.68	8 February 2013	400	1,200
2013/2014	6901030	-5.15	7 January 2014	280	1,500
	1901210	-7.21	5 March 2014	1,500	1,500
	1901217	-6.31	22 April 2014	1,760	1,500
2014/2015	6901030	-7.59	21 February 2015	1,450	1,650
	1901210	-6.93	9 April 2015	1,680	1,650
	1901217	-7.05	18 March 2015	1,530	1,650
2015/2016	6901030	-6.37	16 February 2016	250	1,900

^aThe bold rows represent cases where floats observed convection greater than 800 m. ^bTaken from Yashayaev and Loder (2016) and Yashayaev and Loder (2017).

Despite complex interannual variability in the physics forcing Labrador Sea deep convection (Yashayaev & Loder, 2016), this seasonal cycle is representative of multiple floats for multiple years (Figure 4). Interannual differences in peak saturation anomaly (10% to 24%) depend on spring bloom variability (Frajka-Williams & Rhines, 2010). We address the differences in convective undersaturation in the next

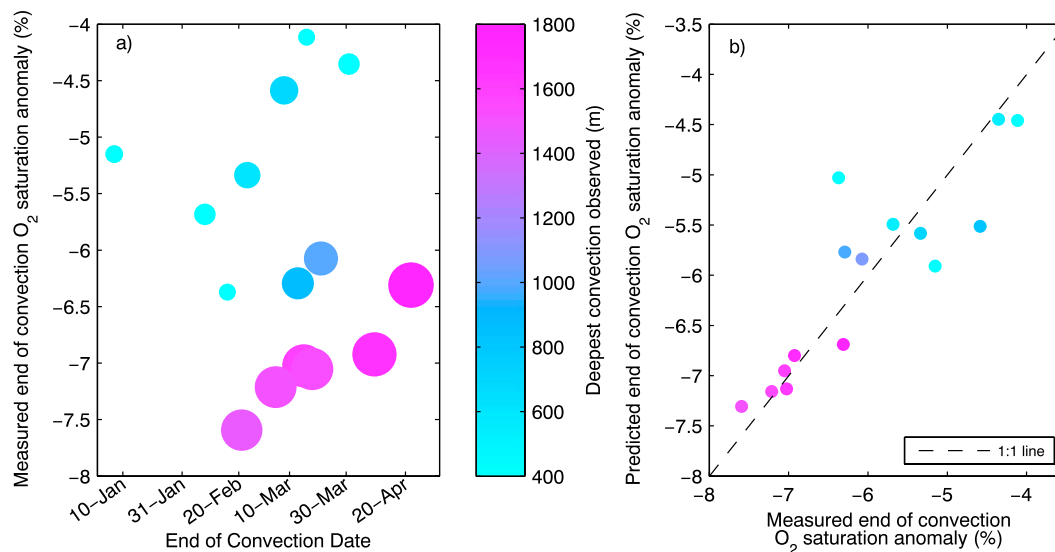


Figure 5. (a) End of convection surface oxygen saturation anomaly (%) as a function of convection end date. The dot color and size represents maximum depth of convection observed by the float (bigger and more pink is deeper; smaller and more blue is shallower). (b) Predicted end of convection oxygen saturation anomaly from equation (6) plotted against float measured end of convection oxygen saturation anomaly. Point color same as (a).

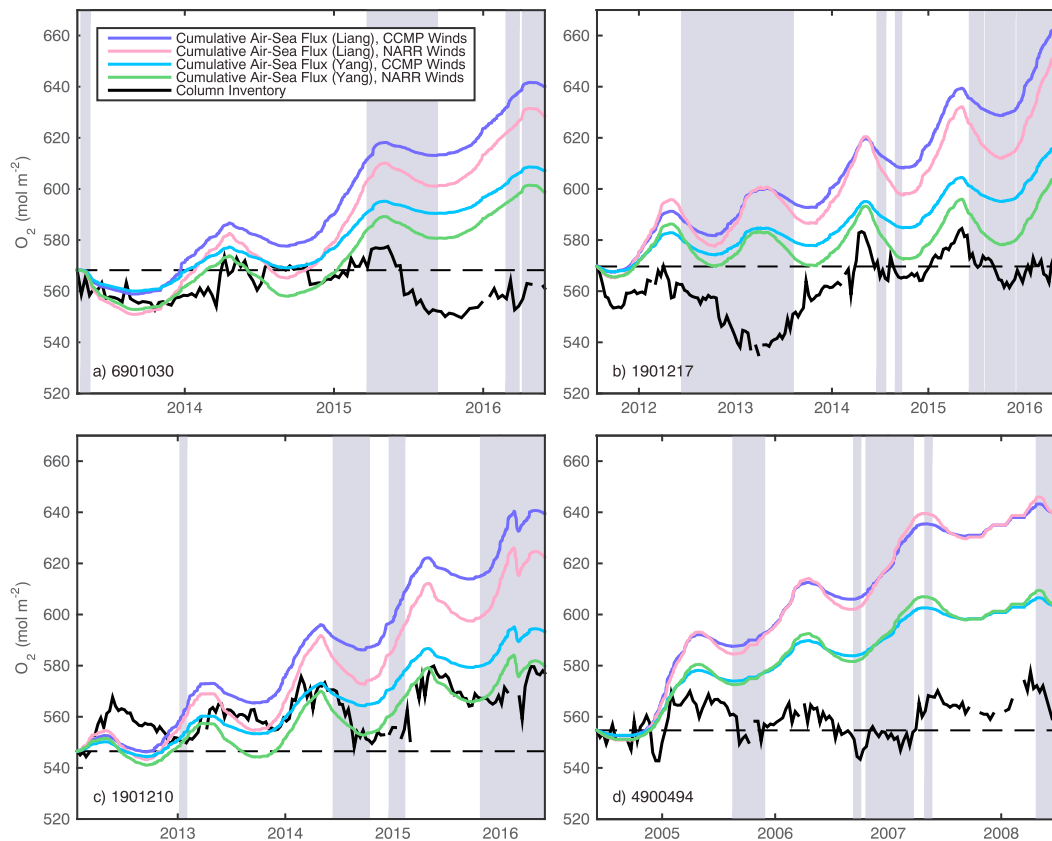


Figure 6. Time series of the cumulative air-sea flux (mol m^{-2}) calculated using the Liang et al. (2013) gas exchange parameterization with cross-calibrated multiplatform (CCMP) winds (purple line) and North American Regional Reanalysis (NARR) winds (pink line) and the Yang et al. (2017) parameterization with CCMP winds (blue line) and NARR winds (green line) compared to the oxygen column inventory from 0 to 1,900 m (solid black line) for four floats (float number indicated in lower left corners). The gray shaded regions represent time periods when floats left the study region (Figure 1). Floats 4900607 and 4900611 are shown in Figure S3.

section, focusing our interpretation on the values within the Labrador Sea, though the oxygen saturation anomaly signal outside of our region of interest is similar (dotted line segments in Figure 4).

4.2. Saturation at the End of Convection

At the end of convection, we found that surface waters were consistently undersaturated at -6.1% to -7.6% in all cases where floats observed convection deeper than 800 m (bold rows in Table 2). We attribute the variation in saturation anomaly to two factors, the date convection ended and the maximum depth of convection.

Floats that observe later convection (either because convection ended later in that year or because the float remained in the convection region longer) have oxygen saturation anomalies closer to equilibrium at the end of convection. For example, in convection events deeper than 1,400 m, the oxygen saturation anomaly at the end of convection is closer to equilibrium when convection ends later (pink and purple dots in Figure 5a). As convection ends later, the undersaturated water has more time to take up oxygen, driving the layer closer to equilibrium. Similarly, Sun et al. (2017) found that modeled oxygen uptake was enhanced by longer convection events.

Floats that happen to observe deeper convective events typically have oxygen saturation anomalies further from equilibrium. Comparing convection events of varying depths but similar end dates shows that deeper convection leads to greater undersaturation (e.g., ~ 15 Mar in Figure 5a). During deeper convection events, a larger volume of undersaturated waters is added to the mixed layer. In addition, the larger volume mixed layer has a longer residence time and cannot approach equilibrium quickly. Conversely, floats in regions and times when convection was shallower have oxygen saturation anomalies closer to equilibrium at the end of convection. With shallower convective events, less of the highly undersaturated water is brought

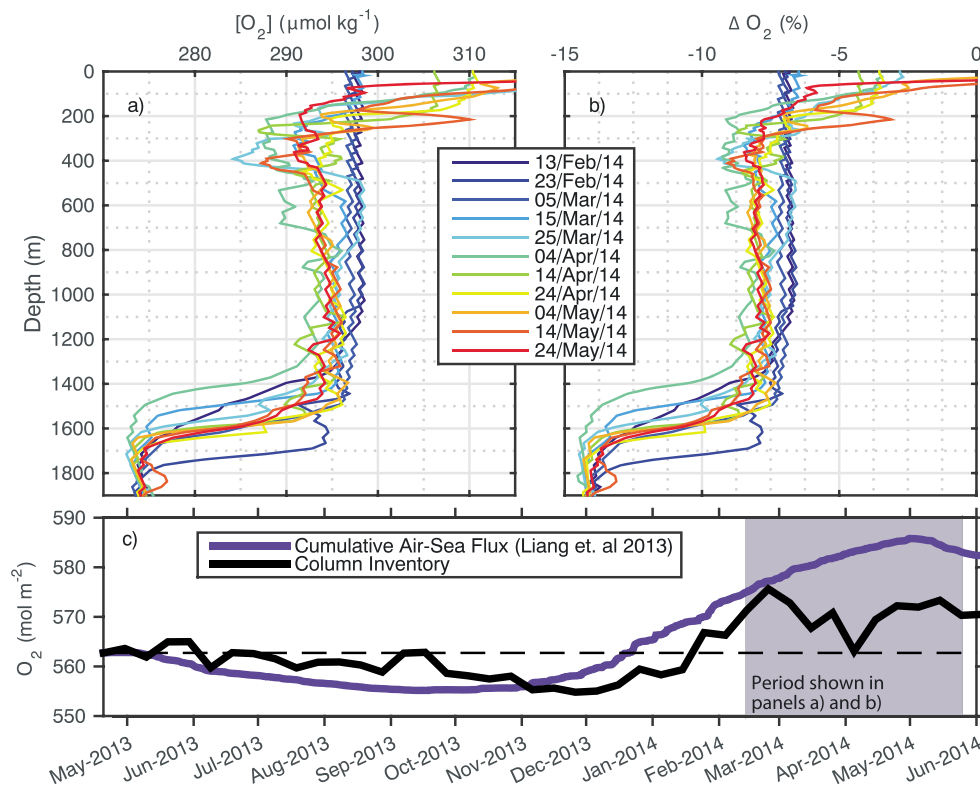


Figure 7. Evolution of (a) oxygen concentration profiles ($\mu\text{mol kg}^{-1}$) and (b) oxygen saturation anomaly profiles (%) during a time period (c, shaded gray region) when the trend in cumulative air-sea flux (mol m^{-2}) (c, solid purple line) based on Liang et al. (2013) and CCMP winds differs greatly from the column inventory (c, solid black line). The jagged nature of the profiles is due to the resolution of data transmitted via satellite for this Argo float.

into the mixed layer, and the smaller volume of water approaches equilibrium faster. For floats not in the region of maximum convection, we observe shallower mixed layers resulting in saturation anomalies closer to equilibrium, -4.1% to -6.2% (light blue dots in Figure 5). Observed end of convection values (Table 2) are often higher than the minimum saturation anomaly in that same winter (Figure 4), likely due to gas exchange bringing oxygen somewhat closer to equilibrium before the end of deep convection.

The end of convection oxygen saturation anomalies we derive are consistent with ship-based measurements from two rare winter cruises in the Labrador Sea: values of -6% to -7% during an early March 1976 cruise with convection to 1,500 m (Clarke and Coote, 1988) and average surface oxygen saturation anomalies of -6.1% during a February–March 1997 cruise also with convection to 1,500 m (Knorr 147 Leg V Hydrographic Data Report).

Comparing our oxygen saturation anomalies to argon enables separation of the biological and physical processes affecting oxygen. Oxygen and argon have very similar solubilities, temperature dependencies, and diffusion rates, such that argon saturation anomalies quantify the impact of physical processes (cooling, atmospheric pressure, and bubbles) on oxygen. Hamme et al. (2017) report argon saturation anomalies in Labrador Sea Water of $-1.26 \pm 0.15\%$. The difference between the oxygen and argon saturation anomalies of approximately -5% to -6.2% represents the deep biological deficit not erased by gas exchange. Convective entrainment of waters with low oxygen concentrations due to respiration is the main reason for oxygen undersaturation in newly convected waters, rather than cooling or low atmospheric pressures.

We derive a predictive relationship for the end of convection oxygen saturation anomaly based on maximum observed convection depth and convection end date using multiple linear regression:

$$\Delta O_2^{\text{predicted}} = -1.9792 \times 10^{-3} \cdot \text{Depth} + 2.0466 \times 10^{-2} \cdot \text{Yearday} - 5.4991 \quad (6)$$

where $\Delta O_2^{\text{predicted}}$ is the predicted end of convection oxygen saturation anomaly (%), Depth is the maximum depth of convection observed by the float (m), and Yearday is the end date of convection expressed as day of

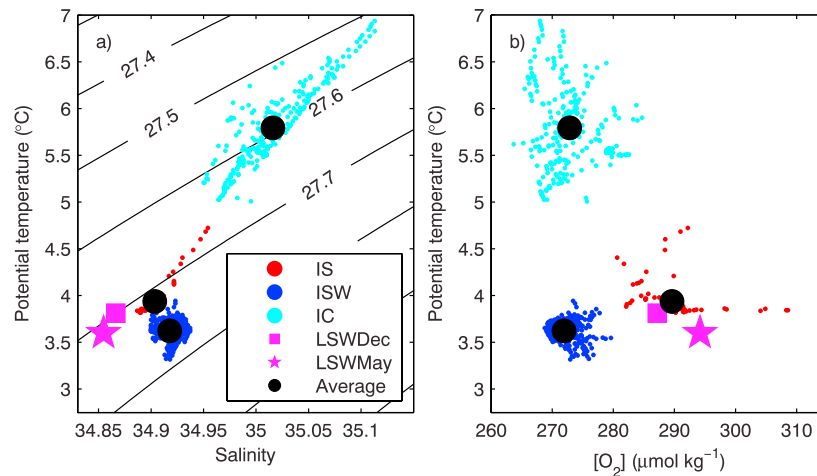


Figure 8. (a) Potential temperature (°C) versus salinity (PSS-78) and (b) potential temperature versus dissolved oxygen ($\mu\text{mol kg}^{-1}$), highlighting the three water masses used to determine the external end-member for the lateral flux analysis. Irminger Sea water (IS, red), Icelandic Slope Water (ISW, blue), and Irminger Current (IC, cyan) have average properties marked by large black circles. The pink star and square denote Labrador Sea Water in May (LSWMay) and December (LSWDec), respectively. Potential density anomaly contours shown in (a).

the year (i.e., 32 for 1 February). This relationship shows high skill in predicting the observed end of convection oxygen saturation anomaly, with an RMSE between the predicted and observed end of convection oxygen saturation anomalies of 0.58% and p -value of 1.92×10^{-4} (Figure 5b).

We considered surface heat fluxes as a predictive variable, estimated from the sum of net shortwave and longwave radiation, and sensible and latent heat fluxes from NCEP/NCAR Reanalysis I (Kalnay et al., 1996). Wintertime surface heat flux did not have as strong a correlation to the end of convection oxygen saturation anomaly as the maximum depth of convection or the end date of convection (Wolf, 2017). Using surface heat flux and maximum depth of convection as predictive variables resulted in an RMSE of 0.75% and p -value of 3.80×10^{-3} , while using surface heat flux and end date resulted in an RMSE of 0.62% and p -value of 4.46×10^{-4} . Wintertime convection in the Labrador Sea depends on both atmospheric forcing and preconditioning of the water column (Schulze et al., 2016; Yashayaev & Loder, 2017). Maximum convection depth and convection end date capture both these factors, while heat flux ignores preconditioning.

Spatial gradients exist within the Labrador Sea during convection. Convective plumes are on the order of 1 km but are short lived due to mesoscale eddies creating homogenous patches on the order of 10 km (Lab Sea Group, 1998; Steffen & D'Asaro, 2002). In addition, the area of maximum heat loss is centered on the southwest region. Since Argo floats drift, each float may not observe the deepest convection event in the region. Table 2 shows that the maximum convection depth observed by some floats is much shallower than the maximum depth from Yashayaev and Loder (2016) and Yashayaev and Loder (2017), who used temperature and salinity from all available Argo floats in the Labrador Sea to determine mixed layer depth. Furthermore, our convection end date is based on individual float observations, while convection elsewhere in the Labrador Sea may end at a different time. The end of convection oxygen saturation anomalies in this study, and the air-sea fluxes and inventories in the next section, are local values observed by specific floats. However, taken together, these local values constrain a range expected for Labrador Sea Water as a whole.

4.3. Air-Sea Flux Versus Inventory

Air-sea oxygen fluxes calculated from either gas exchange parameterization or wind speed product indicate that the Labrador Sea is a net sink for oxygen, but the uncertainty in the net uptake rate is large. Using the Liang et al. (2013) parameterization with CCMP winds, averaged along float trajectories within our study region, resulted in the largest net annual uptake of $22.8 \pm 5.6 \text{ mol m}^{-2} \text{ yr}^{-1}$, while using the Yang et al. (2017) parameterization with NARR winds resulted in the smallest net annual uptake of $11.6 \pm 6.8 \text{ mol m}^{-2} \text{ yr}^{-1}$ (Figure 6 and Table S1 in the supporting information). Bias between wind speed products produces $0.9 \pm 3.1 \text{ mol m}^{-2} \text{ yr}^{-1}$ of the difference in net annual oxygen uptake. However, the wind speed products are more different in the later years, with a $3.1 \pm 0.6 \text{ mol m}^{-2} \text{ yr}^{-1}$ difference for the newer floats (2011 to

2016) compared to $-1.3 \pm 3.1 \text{ mol m}^{-2} \text{ yr}^{-1}$ for the older floats. The Wanninkhof (1992) parameterization, used in many ocean-atmosphere models (Taylor et al., 2012), yields a net oxygen uptake of $5.7 \pm 6.1 \text{ mol m}^{-2} \text{ yr}^{-1}$ but does not include bubble fluxes and therefore underestimates uptake for an insoluble gas like oxygen. Körtzinger et al. (2008) used oxygen data from the K1 mooring in our study region (Figure 1) to estimate a similar lower net annual oxygen uptake of 7.7 to $11.2 \text{ mol m}^{-2} \text{ yr}^{-1}$ using a variety of gas exchange parameterizations, but none included bubble fluxes.

Despite large interannual variability, the annually averaged column-integrated oxygen inventory is near constant, as expected (Stendardo & Gruber, 2012). The column-integrated oxygen inventory from 0 to 1,900 m (black lines in Figure 6) shows clear seasonality, but the inventory returns to approximately the same level year after year. In contrast, time-integrated air sea fluxes from both parameterizations and wind-speed products (colored lines in Figure 6) increase each year. Such a difference between air-sea flux and inventory, if accurate, must be balanced by lateral mixing with waters with a larger oxygen deficit from outside the convective region. In situ respiration is likely not important to balancing the budget, because it could only play a role if significant organic matter was imported from outside the region. In an isolated one-dimensional system, photosynthesis and respiration are reflected in the local air-sea fluxes leading to balanced fluxes over an annual cycle.

We demonstrate that lateral processes play an important role in the Labrador Sea oxygen budget using a clear example from early 2014 during restratification (Figure 7). During this period, surface waters are still undersaturated driving a flux of oxygen into the ocean. Starting 15 Mar 2014, an intrusion of low oxygen waters from outside the convection region at intermediate depths (200–700 m) lowers the oxygen inventory (Figures 7a and 7b). Similar low oxygen water intrusions during the restratification process can be observed for multiple years in the float data (Wolf, 2017). Körtzinger et al. (2004, 2008) and Frajka-Williams et al. (2014) also observe low oxygen water intrusions during restratification. These examples suggest that advection can return oxygen toward lower levels, providing evidence of net air-sea oxygen uptake in the Labrador Sea. Although examples in the restratification period are most obvious, we do not detect a greater tendency for oxygen inventory decrease events directly following restratification compared with later in the year, suggesting that lateral processes act over larger spatial and temporal scales.

To estimate the lateral flux, we quantified the heat gain in the Labrador Sea during the nonconvective period following Straneo (2006). This method compares December temperatures at 200–1,300 m to the previous May, because only lateral exchanges can increase heat during this time when this layer is cutoff from the surface. We find a May-to-December heat gain over all our float data of $1.1 \pm 1.3 \text{ GJ m}^{-2}$, similar to 0.9 GJ m^{-2} from Straneo (2006). From this and temperature estimates of the two end-members (newly convected Labrador Sea Water (LSW) and the warmer water mass), we can determine the proportion of external waters mixed into the central Labrador Sea.

Defining the properties of the warmer water mass creates significant uncertainty. Lateral exchanges between the interior of the Labrador Sea and the surrounding boundary currents and exterior basins are complex (Gelderloos et al., 2011; Katsman et al., 2004; Saenko et al., 2014; van Aken et al., 2011). Constraining the exchange mechanisms is beyond our scope, so we present a simplified calculation assuming the warmer water mass is some combination of Icelandic Slope Water (ISW), Irminger Current (IC), and water from the interior Irminger Sea (IS). Properties of LSW at 200–1,300 m in the central Labrador Sea for May and December were defined from all floats in this study. Properties for ISW, IC, and IS at 200–1,300 m came from floats 1901210 and 6901030 while in the Irminger Basin (Figure S4). IC has low oxygen with a high temperature and salinity signature, lying on a clear temperature-salinity mixing line from LSW May to LSW December (Figure 8). IS also lies close to this mixing line with slightly higher temperature and salinity than LSW December but has oxygen values between LSW May and December. ISW has higher salinity and lower oxygen than LSW but temperature values between LSW May and December and hence does not fall on a temperature-salinity mixing line with them. We considered three scenarios for the warmer water mass responsible for lateral heat gain in the Labrador Sea during the nonconvective period: (1) 100% IC, (2) 100% IS, and (3) 50% ISW, 25% IC, and 25% IS (mixture). We do not consider 100% ISW, since it is colder than LSW December (Figure 8) and cannot be the only source of heat.

From our simplified analysis, we find that lateral mixing and advection can account for a significant fraction of the difference between our cumulative air-sea flux estimates and the oxygen inventory. The fraction of the warmer water mass that must be mixed into the central Labrador Sea to account for the observed heat

gain over May to December is $9.7\% \text{ yr}^{-1}$ (100% IC), $64.0\% \text{ yr}^{-1}$ (100% IS), or $33.4\% \text{ yr}^{-1}$ (mixture). From these fractions and the water mass oxygen concentrations (Figure 8), and assuming lateral fluxes are constant year-round, we calculate an oxygen decrease due to advection of $3.98 \text{ mol m}^{-2} \text{ yr}^{-1}$ (100% IC), $5.64 \text{ mol m}^{-2} \text{ yr}^{-1}$ (100% IS), or $11.34 \text{ mol m}^{-2} \text{ yr}^{-1}$ (mixture), which accounts for 29.5%, 41.9%, or 84.2% of the observed oxygen inventory decrease in the Labrador Sea from May to December, respectively. These estimated lateral fluxes account for a portion of the annual average difference between the cumulative air-sea fluxes and the inventory, which ranges from 10.5 to $23.3 \text{ mol m}^{-2} \text{ yr}^{-1}$. Depending on the choice of the warmer water mass composition, the cumulative combination of this lateral flux and air-sea gas exchange can result in an oxygen budget that resembles the balanced oxygen inventory (Figure S5). This back-of-the-envelope analysis, though uncertain, suggests that advection may dominate the return of oxygen toward greater undersaturation and make the Labrador Sea a region of significant net oxygen uptake.

We also quantify inventories and fluxes for just the winter season, which compare well to other work. Over all observed winters from 1 November to the convection end date for individual floats, the mean column-integrated oxygen inventory change (0 to 1,900 m) was $10.90 \pm 7.96 \text{ mol m}^{-2}$, while the mean air-sea flux ranges from $23.90 \pm 7.94 \text{ mol m}^{-2}$ from Liang et al. (2013) with CCMP winds to $13.58 \pm 4.67 \text{ mol m}^{-2}$ from Yang et al. (2017) with NARR winds. For the 2003/2004 convective period, we measure a 0 to 1,400-m column-integrated oxygen inventory gain of 16.6 mol m^{-2} compared to the 17 mol m^{-2} found by Körtzinger et al. (2004), from the same float data. For the 2014/2015 convective period, we measure a 0 to 1,700-m column-integrated oxygen inventory gain of 21.6 mol m^{-2} from the float closest to the K1 mooring compared to $24.3 \pm 3.4 \text{ mol m}^{-2}$ found by Koelling et al. (2017) using K1 mooring data. Our net air-sea flux during this time ranges from $36.6 \pm 3.8 \text{ mol m}^{-2}$ from Liang et al. (2013) with CCMP winds to $21.6 \pm 2.6 \text{ mol m}^{-2}$ from Yang et al. (2017) with NARR winds.

5. Conclusions

In this study, we found a strong correlation between the end of convection oxygen values in the Labrador Sea and convection depth and end date, with deeper convection and earlier end dates resulting in more undersaturated surface waters. The end of convection oxygen saturation anomaly was -6.1% to -7.6% in all cases with convection deeper than 800 m. Since both the convection depth and end date are easily obtained from standard Argo floats measuring temperature and salinity, the predictive relationship we developed could be used to produce an abundant proxy data set for end of convection saturation anomalies from standard Argo floats. The fairly tight saturation anomaly range (1.5%) in our results demonstrates that the influence of inter-annual variability in convection depth and end date is less important than the overall large undersaturation (order -7%) generated in this region.

Our findings on the degree of oxygen undersaturation after deep convection provide a correction to AOU estimates in Labrador Sea Water and an additional constraint for biogeochemical models and global carbon budgets. A 7% underestimate in surface oxygen, as we found in Labrador Sea Water, would create estimates of AOU that are too high by $24 \mu\text{mol kg}^{-1}$ and of regenerated nutrients from AOU that are too high by $0.13 \mu\text{mol kg}^{-1}$ for phosphate and $2.1 \mu\text{mol kg}^{-1}$ for nitrate, using Redfield ratios from Anderson and Sarmiento (1994), a 12–13% overestimate of regenerated/total nutrient ratios in LSW (Garcia et al., 2014). Increases in interior DIC due to respiration and calcium carbonate dissolution are also estimated from AOU when calculating anthropogenic carbon. A 7% error in surface oxygen would produce an $\sim 14 \mu\text{mol kg}^{-1}$ error in the DIC content attributed to biological sources, using a C:O₂ ratio of 109:170 (Sabine et al., 2004). This error does not create an equivalent error in anthropogenic carbon content, because the ΔC^* method accounts for much of this AOU-induced error in the disequilibrium term (Gruber et al., 1996), but it nevertheless represents a misattribution of the carbon source.

Constraining where and how much oxygen the ocean takes up provides insight into the natural carbon cycle. Rapid decreases in the oxygen inventory during restratification and our simplified estimate of lateral oxygen fluxes argue that horizontal advection provides low oxygen water to the convective region, making the Labrador Sea a region of net oxygen uptake. However, uncertainty in gas exchange parameterizations and in lateral fluxes limits our ability to close the annual oxygen budget and quantify the net annual uptake. Our analysis also exemplifies the dangers of treating Argo profiles in a one-dimensional sense, given that horizontal advection transports oxygenated waters elsewhere or the float itself advects.

Our study highlights the strengths and weaknesses of profiling floats equipped with oxygen sensors. The temporal and spatial coverage of these floats surpasses ship-based measurements. A more expansive float array coverage, like the new Biogeochemical-Argo Program will provide (Biogeochemical-Argo Planning Group, 2016), would resolve regional differences within the convective region and prevent gaps in observing convection by advection of floats outside the region. The majority of our floats showed significant in situ drift, which we corrected to stable deepwater oxygen values. The North Atlantic is particularly suited for this calibration technique, because deep oxygen values are high, such that both surface and deep values are corrected similarly. Extrapolation of the deep calibration to the surface may result in biases in areas where deep stable values are very undersaturated. For newly deployed floats, float modifications that enable in-air oxygen measurements for optode calibration have the potential to produce accurate measurements regardless of study region (Bittig & Körtzinger, 2015; Bushinsky et al., 2016; Johnson et al., 2015).

Acknowledgments

We thank J. Klymak, J. Koelling, K. Johnson, and H. Bittig for helpful discussions. We would like to thank NSERC for funding through the CCAR VITALS network under 433898-2012 to Paul Myers. V. Thierry's contribution to this work was part of the EQUIPEX NAOS project funded by the French National Research Agency (ANR) under reference ANR-10-EQPX-40. Argo data were collected and made freely available by the International Argo Program and the national programs that contribute to it (<http://www.argo.ucsd.edu>, <http://argo.jcommops.org>). The Argo Program is part of the Global Ocean Observing System (<http://doi.org/10.17882/42182#48844>). CCMP Version 2.0 vector wind analyses are produced by Remote Sensing Systems. Data are available at www.remss.com. NCEP Reanalysis data provided by the NOAA/OAR/ESRL PSD, Boulder, Colorado, USA, from their Web site at <http://www.esrl.noaa.gov/psd/>. NARR data provided by the NOAA/OAR/ESRL PSD, Boulder, Colorado, USA, from their Web site at <https://www.esrl.noaa.gov/psd/>.

References

- Anderson, L. A., & Sarmiento, J. L. (1994). Redfield ratios of remineralization determined by nutrient data analysis. *Global Biogeochemical Cycles*, 8(1), 65–80. <https://doi.org/10.1029/93GB03318>
- Argo (2000). Argo float data and metadata from Global Data Assembly Centre (Argo GDAC). SEANOE. <https://doi.org/10.17882/42182#48844> (March 8, 2017 snapshot)
- Atlas, R., Hoffman, R. N., Ardizzone, J., Leidner, S. M., Jusem, J. C., Smith, D. K., & Gombos, D. (2011). A cross-calibrated, multiplatform ocean surface wind velocity product for meteorological and oceanographic applications. *Bulletin of the American Meteorological Society*, 92(2), 157–174. <https://doi.org/10.1175/2010BAMS2946.1>
- Azetsu-Scott, K., Clarke, A., Falkner, K., Hamilton, J., Jones, E. P., Lee, C., et al. (2010). Calcium carbonate saturation states in the waters of the Canadian Arctic Archipelago and the Labrador Sea. *Journal of Geophysical Research*, 115, C11021. <https://doi.org/10.1029/2009JC005917>
- Azetsu-Scott, K., Jones, E. P., Yashayaev, I., & Gershey, R. M. (2003). Time series study of CFC concentrations in the Labrador Sea during deep and shallow convection regimes (1991–2000). *Journal of Geophysical Research*, 108(C11), 3354. <https://doi.org/10.1029/2002JC001317>
- Biogeochemical-Argo Planning Group (2016). The scientific rationale, design and implementation plan for a Biogeochemical-Argo float array. Edited by Ken Johnson and Hervé Claustre. <https://doi.org/10.13155/46601>
- Bittig, H. C., Fiedler, B., Fietzek, P., & Körtzinger, A. (2015). Pressure response of Aanderaa and sea-bird oxygen optodes. *Journal of Atmospheric and Oceanic Technology*, 32(12), 2305–2317. <https://doi.org/10.1175/jtechd-15-0108.1>
- Bittig, H. C., & Körtzinger, A. (2015). Tackling oxygen optode drift: Near-surface and in-air oxygen optode measurements on a float provide an accurate in situ reference. *Journal of Atmospheric and Oceanic Technology*, 32(8), 1536–1543. <https://doi.org/10.1175/jtech-d-14-00162.1>
- Bittig, H. C., & Körtzinger, A. (2017). Technical note: Update on response times, in-air measurements, and in situ drift for oxygen optodes on profiling platforms. *Ocean Science*, 13(1), 1–11. <https://doi.org/10.5194/os-13-1-2017>
- Bittig, H. C., Körtzinger, A., Neill, C., van Ooijen, E., Plant, J. N., Hahn, J., et al. (2018). Oxygen optode sensors: Principle, characterization, calibration, and application in the ocean. *Frontiers in Marine Science*, 4, 429. <https://doi.org/10.3389/fmars.2017.00429>
- Böning, C. W., Behrens, E., Biastoch, A., Getzlaff, K., & Bamber, J. L. (2016). Emerging impact of Greenland meltwater on deepwater formation in the North Atlantic Ocean. *Nature Geoscience*, 9(7), 523–527. <https://doi.org/10.1038/ngeo2740>
- Broecker, W. S., & Peng, T.-H. (1982). *Tracers in the sea*. Palisades, New York: Lamont-Doherty Earth Observatory. [https://doi.org/10.1016/0016-7037\(83\)90075-3](https://doi.org/10.1016/0016-7037(83)90075-3)
- Bushinsky, S. M., Emerson, S. R., Riser, S. C., & Swift, D. D. (2016). Accurate oxygen measurements on modified Argo floats using in situ air calibrations. *Limnology and Oceanography: Methods*, 14(8), 491–505. <https://doi.org/10.1002/lom3.10107>
- Carlson, C. A., Hansell, D. A., Nelson, N. B., Siegel, D. A., Smethie, W. M. J., Khattiwala, S., et al. (2010). Dissolved organic carbon export and subsequent remineralization in the mesopelagic and bathypelagic realms of the North Atlantic basin. *Deep-Sea Research Part II*, 57(16), 1433–1445. <https://doi.org/10.1016/j.dsr2.2010.02.013>
- Clarke, R. A., & Coote, A. R. (1988). The formation of Labrador Sea Water. Part III: The Evolution of Oxygen and Nutrient Concentration. *Journal of Physical Oceanography*, 18(3), 469–480. [https://doi.org/10.1175/1520-0485\(1988\)018%3C0469:TFOLSW%3E2.0.CO;2](https://doi.org/10.1175/1520-0485(1988)018%3C0469:TFOLSW%3E2.0.CO;2)
- Cowie, G. L., Hedges, J. I., Prahl, F. G., & De Lange, G. J. (1995). Elemental and major biochemical changes across an oxidation front in a relict turbidite: A clear-cut oxygen effect. *Geochimica et Cosmochimica Acta*, 59(1), 33–46. [https://doi.org/10.1016/0016-7037\(94\)00329-K](https://doi.org/10.1016/0016-7037(94)00329-K)
- Culbertson, C. H. (1994). Dissolved oxygen, in WOCE Operations Manual, Volume 3, Section 1, Part 3: WHP Operations and Methods, WHP Office Report WHPO 91-1, WOCE Report No. 68/91, Woods Hole Oceanographic Institute, Woods Hole, Massachusetts.
- D'Asaro, E. A., & McNeil, C. (2013). Calibration and stability of oxygen sensors on autonomous floats. *Journal of Atmospheric and Oceanic Technology*, 30(8), 1896–1906. <https://doi.org/10.1175/JTECH-D-12-00222.1>
- DeGrandpre, M. D., Körtzinger, A., Send, U., Wallace, D. W. R., & Bellerby, R. G. J. (2006). Uptake and sequestration of atmospheric CO₂ in the Labrador Sea deep convection region. *Geophysical Research Letters*, 33, L21503. <https://doi.org/10.1029/2006GL026881>
- Dickson, A. G., Sabine, C. L., & Christian, J. R. (2007). *Guide to best practices for ocean CO₂ measurements*, PICES Special Publication 3 (p. 191). Sidney, British Columbia: North Pacific Marine Science Organization. <http://hdl.handle.net/11329/249>
- Dickson, R. R., Rudels, B., Dye, S., Karcher, M., Meincke, J., & Yashayaev, I. (2007). Current estimates of freshwater flux through Arctic and subarctic seas. *Progress in Oceanography*, 73(3–4), 210–230. <https://doi.org/10.1016/j.pocean.2006.12.003>
- Duteil, O., Koeve, W., Oschlies, A., Aumont, O., Bianchi, D., Bopp, L., et al. (2012). Preformed and regenerated phosphate in ocean general circulation models: Can right total concentrations be wrong? *Biogeosciences*, 9(5), 1797–1807. <https://doi.org/10.5194/bg-9-1797-2012>
- Duteil, O., Koeve, W., Oschlies, A., Bianchi, D., Galbraith, E., Kriest, I., & Matear, R. (2013). A novel estimate of ocean oxygen utilisation points to a reduced rate of respiration in the ocean interior. *Biogeosciences*, 10(11), 7723–7738. <https://doi.org/10.5194/bg-10-7723-2013>
- Emerson, S., & Bushinsky, S. (2016). The role of bubbles during air-sea gas exchange. *Journal of Geophysical Research: Oceans*, 121, 4360–4376. <https://doi.org/10.1002/2016JC011744>
- Ferrell, R. T., & Himmelblau, D. M. (1967). Diffusion coefficients of nitrogen and oxygen in water. *Journal of Chemical & Engineering Data*, 12(1), 111–115. <https://doi.org/10.1021/je60032a036>

- Frajka-Williams, E., & Rhines, P. B. (2010). Physical controls and interannual variability of the Labrador Sea spring phytoplankton bloom in distinct regions. *Deep Sea Research Part I*, 57(4), 541–552. <https://doi.org/10.1016/j.dsr.2010.01.003>
- Frajka-Williams, E., Rhines, P. B., & Eriksen, C. C. (2014). Horizontal stratification during deep convection in the Labrador Sea. *Journal of Physical Oceanography*, 44(1), 220–228. <https://doi.org/10.1175/JPO-D-13-069.1>
- Garcia, H. E., & Gordon, L. I. (1992). Oxygen solubility in seawater: Better fitting equations. *Limnology and Oceanography*, 37(6), 1307–1312. <https://doi.org/10.4319/lo.1992.37.6.1307>
- Garcia, H. E., & Gordon, L. I. (1993). Erratum: Oxygen solubility in seawater: Better fitting equations. *Limnology and Oceanography*, 38, 656.
- Garcia, H. E., Locarnini, R. A., Boyer, T. P., Antonov, J. I., Baranova, O. K., Zweng, M. M., et al. (2014). In S. Levitus & A. Mishonov Technical (Eds.), *World Ocean Atlas 2013, volume 4: Dissolved inorganic nutrients (phosphate, nitrate, silicate)* (Vol. 76, p. 25). Silver Spring, MD: NOAA Atlas NESDIS.
- Gelderloos, R., Katsman, C. A., & Drijhout, S. S. (2011). Assessing the roles of three eddy types in restratifying the Labrador Sea after deep convection. *Journal of Physical Oceanography*, 41(11), 2102–2119. <https://doi.org/10.1175/JPO-D-11-054.1>
- Gilbert, D. (2017). Environmental science: Oceans lose oxygen. *Nature*, 542(7641), 303–304. <https://doi.org/10.1038/542303a>
- Gilbert, D., Rabalais, N. N., Diaz, R. J., & Zhang, J. (2010). Evidence for greater oxygen decline rates in the coastal ocean than in the open ocean. *Biogeosciences*, 7(7), 2283–2296. <https://doi.org/10.5194/bg-7-2283-2010>
- Gruber, N., Sarmiento, J. L., & Stocker, T. F. (1996). An improved method for detecting anthropogenic CO₂ in the oceans. *Global Biogeochemical Cycles*, 10(4), 809–837. <https://doi.org/10.1029/96GB01608>
- Hamme, R., Emerson, S. R., Severinghaus, J. P., Long, M. C., & Yashayaev, I. (2017). Using noble gas measurements to derive air-sea process information and predict physical gas saturations. *Geophysical Research Letters*, 44, 9901–9909. <https://doi.org/10.1002/2017GL075123>
- Hamme, R. C., Berry, J. E., Klymak, J. M., & Denman, K. L. (2015). In situ O₂ and N₂ measurements detect deep-water renewal dynamics in seasonally-anoxic Saanich Inlet. *Continental Shelf Research*, 106, 107–117. <https://doi.org/10.1016/j.csr.2015.06.012>
- Holte, J., Gilson, J., Talley, L., & Roemmich, D. (2016). Argo mixed layers, Scripps Institution of Oceanography/UCSD. Retrieved from <http://mixedlayer.ucsd.edu>, (accessed [17/02/2017]).
- Ito, T., Follows, M. J., & Boyle, E. A. (2004). Is AOU a good measure of respiration in the oceans? *Geophysical Research Letters*, 31, L17305. <https://doi.org/10.1029/2004GL020900>
- Johnson, K. S., Berelson, W. M., Boss, E. S., Chase, Z., Claustre, H., Emerson, S. R., et al. (2009). Observing biogeochemical cycles at global scales with profiling floats and gliders: Prospects for a global array. *Oceanography*, 22(3), 216–225. <https://doi.org/10.5670/oceanog.2009.81>
- Johnson, K. S., Plant, J. N., Riser, S. C., & Gilbert, D. (2015). Air oxygen calibration of oxygen optodes on a profiling float array. *Journal of Atmospheric and Oceanic Technology*, 32(11), 2160–2172. <https://doi.org/10.1175/jtech-d-15-0101.1>
- Kalnay, E., Kanamitsu, M., Kistler, R., Collins, W., Deaven, D., Gandin, L., et al. (1996). The NCEP/NCAR 40-year reanalysis project. *Bulletin of the American Meteorological Society*, 77(3), 437–471. [https://doi.org/10.1175/1520-5210477\(1996\)077%3C0437:TNYRP%3E2.0.CO;2](https://doi.org/10.1175/1520-5210477(1996)077%3C0437:TNYRP%3E2.0.CO;2)
- Katsman, C. A., Spall, M. A., & Pickart, R. S. (2004). Boundary current eddies and their role in the restratification of the Labrador Sea. *Journal of Physical Oceanography*, 34(9), 1967–1983. [https://doi.org/10.1175/1520-0485\(2004\)034%3C1967:BCAETR%3E2.0.CO;2](https://doi.org/10.1175/1520-0485(2004)034%3C1967:BCAETR%3E2.0.CO;2)
- Keeling, R. F., Körtzinger, A., & Gruber, N. (2010). Ocean deoxygenation in a warming world. *Annual Review of Marine Science*, 2(1), 199–229. <https://doi.org/10.1146/annurev.marine.010908.163855>
- Khatiwala, S., Tanhua, T., Mikaloff Fletcher, S., Gerber, M., Doney, S. C., Graven, H. D., et al. (2013). Global ocean storage of anthropogenic carbon. *Biogeosciences*, 10(4), 2169–2191. <https://doi.org/10.5194/bg-10-2169-2013>
- Kieke, D., & Yashayaev, I. (2015). Studies of Labrador Sea Water formation and variability in the subpolar North Atlantic in the light of international partnership and collaboration. *Progress in Oceanography*, 132, 220–232. <https://doi.org/10.1016/j.pocean.2014.12.010>
- Kihm, C., & Körtzinger, A. (2010). Air-sea gas transfer velocity for oxygen derived from float data. *Journal of Geophysical Research: Oceans*, 115, C12003. <https://doi.org/10.1029/2009JC006077>
- Klots, C. E. (1961). Effect of hydrostatic pressure upon the solubility of gases. *Limnology and Oceanography*, 6(3), 365–366. <https://doi.org/10.4319/lo.1961.6.3.0365>
- Koelling, J., Send, U., Karstensen, J., & Wallace, D. W. R. (2017). Intense uptake of O₂ during 2014–15 winter convection in the Labrador Sea. *Geophysical Research Letters*, 44, 7855–7864. <https://doi.org/10.1002/2017GL073933>
- Körtzinger, A., Schimanski, J., & Send, U. (2005). High quality oxygen measurements from profiling floats: A promising new technique. *Journal of Atmospheric and Oceanic Technology*, 22(3), 302–308. <https://doi.org/10.1175/jtech1701.1>
- Körtzinger, A., Schimanski, J., Send, U., & Wallace, D. (2004). The ocean takes a deep breath. *Science*, 306(5700), 1337–1337. <https://doi.org/10.1126/science.1102557>
- Körtzinger, A., Send, U., Wallace, D. W. R., Kartensen, J., & DeGrandpre, M. (2008). Seasonal cycle of O₂ and pCO₂ in the central Labrador Sea: Atmospheric, biological, and physical implications. *Global Biogeochemical Cycles*, 22, GB1014. <https://doi.org/10.1029/2007GB003029>
- Lab Sea Group (1998). The Labrador Sea Deep Convection Experiment. *Bulletin of the American Meteorology Society*, 79(10), 2033–2058. [https://doi.org/10.1175/1520-0477\(1998\)079%3C2033:TLSDCE%3E2.0.CO;2](https://doi.org/10.1175/1520-0477(1998)079%3C2033:TLSDCE%3E2.0.CO;2)
- Lavender, K. L., Davis, R. E., & Owens, W. B. (2002). Observations of open-ocean deep convection in the Labrador Sea from subsurface floats. *Journal of Physical Oceanography*, 32(2), 511–526. [https://doi.org/10.1175/1520-0485\(2002\)032%3C0511:oooodc%3E2.0.co;2](https://doi.org/10.1175/1520-0485(2002)032%3C0511:oooodc%3E2.0.co;2)
- Lazier, J., Hendry, R., Clarke, A., Yashayaev, I., & Rhines, P. (2002). Convection and restratification in the Labrador Sea, 1990–2000. *Deep Sea Research Part I*, 49(10), 1819–1835. [https://doi.org/10.1016/S0967-0637\(02\)00064-X](https://doi.org/10.1016/S0967-0637(02)00064-X)
- Liang, J.-H., Deutsch, C., McWilliams, J. C., Baschek, B., Sullivan, P. P., & Chiba, D. (2013). Parameterizing bubble-mediated air-sea gas exchange and its effect on ocean ventilation. *Global Biogeochemical Cycles*, 27, 894–905. <https://doi.org/10.1002/gbc.20080>
- Lilly, J. M., Rhines, P. B., Schott, F., Lavender, K., Lazier, J., Send, U., & D'Asaro, E. (2003). Observations of the Labrador Sea eddy field. *Progress in Oceanography*, 59(1), 75–176. <https://doi.org/10.1016/j.pocean.2003.08.013>
- Martz, T. R., Johnson, K. S., & Riser, S. C. (2008). Ocean metabolism observed with oxygen sensors on profiling floats in the South Pacific. *Limnology and Oceanography*, 53(5part2), 2094–2111. https://doi.org/10.4319/lo.2008.53.5_part_2.2094
- Mesinger, F., DiMego, G., Kalnay, E., Mitchell, K., Shafran, P. C., Ebisuzaki, W., et al. (2006). North American Regional Reanalysis. *Bulletin of the American Meteorological Society*, 87(3), 343–360. <https://doi.org/10.1175/BAMS-87-3-343>
- Najjar, R. G., & Keeling, R. F. (1997). Analysis of the mean annual cycle of the dissolved oxygen anomaly in the World Ocean. *Journal of Marine Research*, 55(1), 117–151. <https://doi.org/10.1357/0022240973224481>
- Pickart, R. S., Torres, D. J., & Clarke, R. A. (2002). Hydrography of the Labrador Sea during active convection. *Journal of Physical Oceanography*, 32(2), 428–457. [https://doi.org/10.1175/1520-0485\(2002\)032%3C0428:HOTLSD%3E2.0.CO;2](https://doi.org/10.1175/1520-0485(2002)032%3C0428:HOTLSD%3E2.0.CO;2)
- Piron, A., Thierry, V., Mercier, H., & Caniaux, G. (2016). Argo float observations of basin-scale deep convection in the Irminger sea during winter 2011–2012. *Deep Sea Research Part I*, 109, 76–90. <https://doi.org/10.1016/j.dsr.2015.12.012>
- Piron, A., Thierry, V., Mercier, H., & Caniaux, G. (2017). Gyre scale deep convection in the subpolar North-Atlantic Ocean during winter 2014–2015. *Geophysical Research Letters*, 44, 1439–1447. <https://doi.org/10.1002/2016GL071895>

- Plant, J. N., Johnson, K. S., Sakamoto, C. M., Jannasch, H. W., Coletti, L. J., Riser, S. C., & Swift, D. D. (2016). Net community production at ocean station papa observed with nitrate and oxygen sensors on profiling floats. *Global Biogeochemical Cycles*, *30*, 859–879. <https://doi.org/10.1002/2015GB005349>
- Prakash, S., Balakrishnan Nair, T. M., Udaya Bhaskar, T. V. S., Prakash, P., & Gilbert, D. (2012). Oxycline variability in the central Arabian Sea: An Argo-oxygen study. *Journal of Sea Research*, *71*, 1–8. <https://doi.org/10.1016/j.seares.2012.03.003>
- Riser, S. C., & Johnson, K. S. (2008). Net production of oxygen in the subtropical ocean. *Nature*, *451*(7176), 323–325. <https://doi.org/10.1038/Nature06441>
- Sabine, C. L., Feely, R. A., Gruber, N., Key, R. M., Lee, K., Bullister, J. L., et al. (2004). The oceanic sink for anthropogenic CO₂. *Science*, *305*(5682), 367–371. <https://doi.org/10.1126/science.1097403>
- Saenko, O. A., Dupont, F., Yang, D., Myers, P. G., Yashayaev, I., & Smith, G. C. (2014). Role of resolved and parameterized eddies in the Labrador Sea balance of heat and buoyancy. *Journal of Physical Oceanography*, *44*(12), 3008–3032. <https://doi.org/10.1175/JPO-D-14-0041.1>
- Schulze, L. M., Pickart, R. S., & Moore, G. W. K. (2016). Atmospheric forcing during active convection in the Labrador Sea and its impact on mixed-layer depth. *Journal of Geophysical Research: Oceans*, *121*, 6978–6992. <https://doi.org/10.1002/2015JC011607>
- Sharqawy, M. H., Lienhard V, J. H., & Zubair, S. M. (2010). Thermophysical properties of seawater: A review of existing correlations and data. *Desalination and Water Treatment*, *16*(1-3), 354–380. <https://doi.org/10.5004/dwt.2010.1079>
- Stanley, R., Jenkins, W., Lott, D., & Doney, S. (2009). Noble gas constraints on air-sea gas exchange and bubble fluxes. *Journal of Geophysical Research*, *114*, C11020. <https://doi.org/10.1029/2009JC005396>
- Steffen, E. L., & D'Asaro, E. A. (2002). Deep convection in the Labrador Sea as observed by Lagrangian floats. *Journal of Physical Oceanography*, *32*(2), 475–492. [https://doi.org/10.1175/1520-0485\(2002\)032%3C0475:DCITLS%3E2.0.CO;2](https://doi.org/10.1175/1520-0485(2002)032%3C0475:DCITLS%3E2.0.CO;2)
- Steinfeldt, R., Rhein, M., Bullister, J. L., & Tanhua, T. (2009). Inventory changes in anthropogenic carbon from 1997–2003 in the Atlantic Ocean between 20°S and 65°N. *Global Biogeochemical Cycles*, *23*, GB3010. <https://doi.org/10.1029/2008GB003311>
- Stendardo, I., & Gruber, N. (2012). Oxygen trends over five decades in the North Atlantic. *Journal of Geophysical Research*, *117*, C11004. <https://doi.org/10.1029/2012JC007909>
- Straneo, F. (2006). Heat and freshwater transport through the central Labrador Sea. *Journal of Physical Oceanography*, *36*(4), 606–628. <https://doi.org/10.1175/JPO2875.1>
- Sun, D., Ito, T., & Bracco, A. (2017). Oceanic uptake of oxygen during deep convection events through diffusive and bubble mediated gas exchange. *Global Biogeochemical Cycles*, *31*, 1579–1591. <https://doi.org/10.1002/2017GB005716>
- Takeshita, Y., Martz, T. R., Johnson, K. S., Plant, J. N., Gilbert, D., Riser, S. C., et al. (2013). A climatology-based quality control procedure for profiling float oxygen data. *Journal of Geophysical Research: Oceans*, *118*, 5640–5650. <https://doi.org/10.1002/jgrc.20399>
- Taylor, K. E., Stouffer, R. J., & Meehl, G. A. (2012). An overview of cmip5 and the experiment design. *Bulletin of the American Meteorological Society*, *93*, 485–498. <https://doi.org/10.1175/BAMS-D-11-00094.1>
- Tengberg, A., Hovdenes, J., Andersson, H., Brocandel, O., Diaz, R., Hebert, D., & Stangelmayer, A. (2006). Evaluation of a lifetime-based optode to measure oxygen in aquatic systems. *Limnology and Oceanography: Methods*, *4*(2), 7–17. <https://doi.org/10.4319/lom.2006.4.7>
- Thierry, V., Bittig, H., Gilbert, D., Kobayashi, T., Schmid, C., & Kanako, S. (2016). *Processing Argo oxygen data at the DAC level cookbook*. Plouzané: LPO-lfremer. <https://doi.org/10.13155/39795>
- Thierry, V., Gilbert, D., Kobayashi, T., & Schmid, C. (2013). Processing Argo oxygen data at the DAC level, version 1.3. Argo data management (20 pp.). Retrieved from http://www.argodatamgt.org/content/download/16300/106561/file/ARGO_oxygen_proposition_v1p3.pdf
- Uchida, H., Kawano, T., Kaneko, I., & Fukasawa, M. (2008). In situ calibration of optode-based oxygen sensors. *Journal of Atmospheric and Oceanic Technology*, *25*(12), 2271–2281. <https://doi.org/10.1175/2008JTECHO549.1>
- Vagle, S., McNeil, C., & Steiner, N. (2010). Upper ocean bubble measurements from the NE Pacific and estimates of their role in air-sea gas transfer of the weakly soluble gases nitrogen and oxygen. *Journal of Geophysical Research*, *115*, C12054. <https://doi.org/10.1029/2009JC005990>
- van Aken, H. M., de Jong, M. F., & Yashayaev, I. (2011). Decadal and multi-decadal variability of Labrador Sea Water in the north-western North Atlantic Ocean derived from tracer distributions: Heat budget, ventilation, and advection. *Deep Sea Research Part I*, *58*(5), 505–523. <https://doi.org/10.1016/j.dsr.2011.02.008>
- Wanninkhof, R. (1992). Relationship between wind speed and gas exchange over the ocean. *Journal of Geophysical Research*, *97*(C5), 7373–7382. <https://doi.org/10.1029/92JC00188>
- Wentz, F. J., Scott, J., Hoffman, R., Leidner, M., Atlas, R., & Ardizzone, J. (2015). Remote Sensing Systems Cross-Calibrated Multi-Platform (CCMP) 6-hourly ocean vector wind analysis product on 0.25 deg grid, Version 2.0. Remote Sensing Systems, Santa Rosa, CA. Retrieved from www.remss.com/measurements/ccmp. [Accessed 19 Dec 2016].
- Wolf, M. K. (2017). Oxygen saturation surrounding deep-water formation events in the Labrador Sea from Argo-O₂ data, (Master's thesis). Retrieved from [UVicSpace]. (<https://dspace.library.uvic.ca/handle/1828/8401>). Victoria, BC: University of Victoria
- Woolf, D. K. (1997). Bubbles and their role in gas exchange. In P. S. Liss & R. A. Duce (Eds.), *The sea surface and global change* (pp. 173–206). New York: Cambridge University Press. <https://doi.org/10.1017/CBO9780511525025.007>
- Woolf, D. K., & Thorpe, S. (1991). Bubbles and the air-sea exchange of gases in near saturation conditions. *Journal of Marine Research*, *49*(3), 435–466. <https://doi.org/10.1357/002224091784995765>
- Wu, Y. S., Platt, T., Tang, C. C. L., & Sathyendranath, S. (2008). Regional differences in the timing of the spring bloom in the Labrador Sea. *Marine Ecology Progress Series*, *355*, 9–20. <https://doi.org/10.3354/meps07233>
- Yang, B., Emerson, S. R., & Bushinsky, S. M. (2017). Annual net oxygen production in the subtropical Pacific Ocean from in situ oxygen measurements on profiling floats. *Global Biogeochemical Cycles*, *31*, 728–744. <https://doi.org/10.1002/2016GB005545>
- Yashayaev, I. (2007). Hydrographic changes in the Labrador Sea, 1960–2005. *Progress in Oceanography*, *73*(3–4), 242–276. <https://doi.org/10.1016/j.pocean.2007.04.015>
- Yashayaev, I., Bersch, M., & vanAken, H. M. (2007). Spreading of the Labrador Sea Water to the Irminger and Iceland basins. *Geophysical Research Letters*, *34*, L10602. <https://doi.org/10.1029/2006GL028999>
- Yashayaev, I., & Loder, J. W. (2016). Recurrent replenishment of Labrador Sea Water and associated decadal-scale variability. *Journal of Geophysical Research: Oceans*, *121*, 8095–8114. <https://doi.org/10.1002/2016JC012046>
- Yashayaev, I., & Loder, J. W. (2017). Further intensification of deep convection in the Labrador Sea in 2016. *Geophysical Research Letters*, *44*, 1429–1438. <https://doi.org/10.1002/2016GL071668>
- Yashayaev, I., vanAken, H. M., Holliday, N. P., & Bersch, M. (2007). Transformation of the Labrador Sea Water in the subpolar North Atlantic. *Geophysical Research Letters*, *34*, L22605. <https://doi.org/10.1029/2007GL031812>
- Zimmerman, S., McKee, T. K., Pickart, R. S., & Smethie, W. M. (2000). Knorr 147 leg V hydrographic data report: Labrador Sea Deep Convection Experiment, WHOI-2000-05, Woods Hole Oceanographic Institute, Woods Hole, Massachusetts. <https://doi.org/10.1575/1912/58>

Erratum

In the originally published version of this article, the quality of the figures in the Supporting Information was poor. The quality of the figures has since been corrected, and this version may be considered the authoritative version of record.